

PAPER • OPEN ACCESS

Finite-time correlations boost large voltage angle fluctuations in electric power grids

To cite this article: Melvyn Tyloo *et al* 2023 *J. Phys. Complex.* **4** 015006

Manuscript version: Accepted Manuscript

Accepted Manuscript is “the version of the article accepted for publication including all changes made as a result of the peer review process, and which may also include the addition to the article by IOP Publishing of a header, an article ID, a cover sheet and/or an ‘Accepted Manuscript’ watermark, but excluding any other editing, typesetting or other changes made by IOP Publishing and/or its licensors”

This Accepted Manuscript is© .



Original content from this work may be used under the terms of the [Creative Commons Attribution 4.0 license](https://creativecommons.org/licenses/by/4.0/). Any further distribution of this work must maintain attribution to the author(s) and the title of the work, journal citation and DOI.

View the [article online](#) for updates and enhancements.

Finite-time Correlations Boost Large Voltage Angle Fluctuations in Electric Power Grids

Melvyn Tyloo^{1,2,3}, Jason Hindes⁴, and Philippe Jacquod^{2,5}

¹*Theoretical Division, Los Alamos National Laboratory, Los Alamos, NM 87545 USA.*

²*Center for Nonlinear Studies (CNLS), Los Alamos National Laboratory, Los Alamos, NM 87545, USA*

³*Department of Quantum Matter Physics, University of Geneva, CH-1211 Geneva, Switzerland*

⁴*U.S. Naval Research Laboratory, Washington, DC 20375, USA*

⁵*School of Engineering, University of Applied Sciences of Western Switzerland HES-SO CH-1951 Sion, Switzerland*

(Dated: January 8, 2023)

Decarbonization in the energy sector has been accompanied by an increased penetration of new renewable energy sources in electric power systems. Such sources differ from traditional productions in that, first, they induce larger, undispachable fluctuations in power generation and second, they lack inertia. Recent measurements have indeed reported long, non-Gaussian tails in the distribution of local voltage frequency data. Large frequency deviations may induce grid instabilities, leading in worst-case scenarios to cascading failures and large-scale blackouts. In this manuscript, we investigate how correlated noise disturbances, characterized by the cumulants of their distribution, propagate through meshed, high-voltage power grids. For a single source of fluctuations, we show that long noise correlation times boost non-Gaussian voltage angle fluctuations so that they propagate similarly to Gaussian fluctuations over the entire network. However, they vanish faster, over short distances if the noise fluctuates rapidly. We furthermore demonstrate that a Berry-Esseen theorem leads to the vanishing of non-Gaussianities as the number of uncorrelated noise sources increases. Our predictions are corroborated by numerical simulations on realistic models of power grids.

I. INTRODUCTION

The fight against climate change is arguably the biggest challenge currently facing humankind [1]. Globally increasing atmospheric and oceanic temperatures have been directly related to the emission of greenhouse gases [2]. Therefore, key to mitigating climate changes is our ability to reduce emissions of such gases. Of particular interest is carbon dioxide, because of its large emission volumes and century-long lifetime in the atmosphere. Decarbonization, i.e. the reduction of carbon dioxide emissions from human activities, requires a fast, fundamental shift to renewable, low-carbon energy sources and a systematic electrification of the energy sector. This will affect the operation of AC electric power grids as both productions and consumptions will change [3]. In particular, higher penetration of renewable energy sources means fluctuating and uncertain power productions [4], as well as reduced electromechanical inertia [5, 6], which impacts dynamic properties of power systems. It is expected – and in fact already observed – that future power grids will be subjected more often to stronger external perturbations to which they may respond more strongly [7, 8].

AC power grids are technological entities that can be modeled as network-coupled dynamical systems. Since they operate according to market rules, it is often difficult to obtain true, reliable data on their operational state. Only recently has it been possible to get access to sufficiently large, statistically significant voltage frequency datasets. Analyses of these datasets have emphasized the non-Gaussian nature of frequency fluctuations in AC power grids [9–12], with distributions ex-

hibiting long tails and large increments. The source of these large deviations is often attributed to the presence of new renewable sources of energy [4, 9, 13, 14]. Large frequency deviations are an important risk factor for the stability and hence the operational safety of present and future AC electric power systems. It is therefore of the utmost importance to understand how non-Gaussian disturbances propagate through electric networks. Many recent papers have investigated the propagation of disturbances originating from fluctuating power feed-in into complex, meshed power grids [9, 14–22]. However, most of them considered either non-noisy, monochromatic excitations or Gaussian-distributed noise, with two notable exceptions. First, Ref. [9] showed analytically for a one-dimensional system that the variance of noise-induced frequency fluctuations decays exponentially away from its feed-in source. Numerical investigations further indicated that this decay seems to hold for meshed graphs as well. Furthermore, the frequency kurtosis was numerically observed to exhibit a slower, possibly power-law decay. Second, Ref. [14] conjectured that the structure of power grids amplifies non-Gaussianities in power feed-in. Different noise probability distributions have been considered, yet the influence of fundamental noise characteristics such as correlation time, or the presence of multiple, independent noise sources has been neglected so far. Below we show that these characteristics are indeed key to understanding how non-Gaussian fluctuations of voltage angles propagate through high-voltage power grids.

The short-time dynamics of power grids is commonly modelled by the swing equations [5], which are nonlinear, damped wave equations on discrete networks. Source terms, representing fluctuating power feed-in, generate

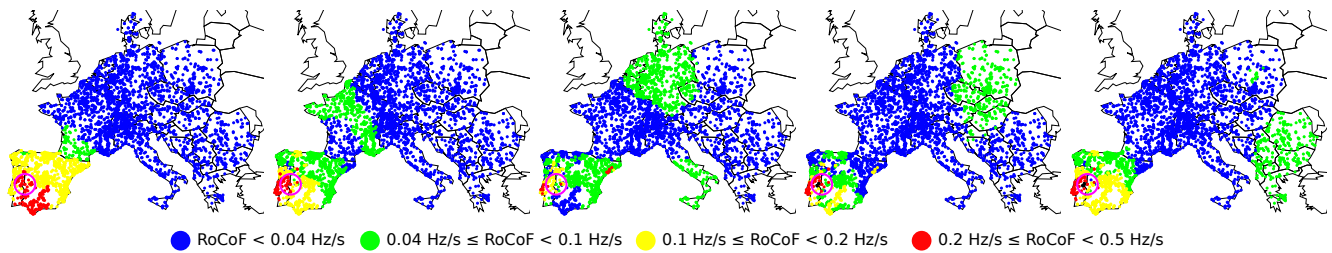


FIG. 1. Calculated spatio-temporal evolution of the voltage angle disturbance across the synchronous grid of continental Europe. Color-plotted are the local Rates of Change of Frequency (RoCoF, defined on the i^{th} node as $\partial_t^2 \theta_i(t)$) for an abrupt power loss of $\delta P = 900$ MW in the Iberian Peninsula (location indicated by the pink circle). Panels correspond to snapshots giving the maximal RoCoF over time intervals 0-0.5[s], 0.5-1[s], 1-1.5[s], 1.5-2[s] and 2-2.5[s] from left to right.

voltage angle and frequency waves that spread through the system. In this manuscript we investigate the propagation of such waves through realistic high-voltage power grids and characterize the noisy source terms by the cumulants of their distributions and by their correlation time τ_0 . Given a single, or several sources of non-Gaussian noise, we calculate the first four cumulants of the voltage angle distribution at any node i on the power grid, over the distribution of the noise injected at one or several nodes. Non-Gaussianities are quantified by nonzero third and fourth cumulants – skewness and kurtosis. We are particularly interested in finding how far they propagate away from the noise sources, and what is their fate in the presence of multiple independent sources of noise. First, we find that non-Gaussianities in noise disturbances propagate differently, depending on the relation between τ_0 and the intrinsic network timescales. When τ_0 is the shortest time scale, non-Gaussianities disappear over short distances relative to Gaussian fluctuations, while when τ_0 is the longest time scale, they propagate through the whole system just like Gaussian fluctuations do, independently of the distribution of inertia. This network-wide propagation of non-Gaussianities is distinct from and goes beyond the bulk, low-frequency response reported in Refs. [20] and [7]. This is what happens when a single noise source is present. Second, from a Berry-Esseen theorem we show that, for identically but independently distributed sources of noise, non-Gaussianities disappear with the number of noise sources in both asymptotics of short and long τ_0 . Our analytical results are corroborated by numerical simulations on realistic high-voltage power grids. Numerics further show that our analytical conclusions regarding voltage angles also apply to voltage frequencies.

Compared to earlier works on noise propagation in complex synchronous networks of oscillators and meshed power grids [9, 14–21, 23–28], our manuscript (i) goes beyond the white-noise limit, and includes in particular regimes of long noise correlation time that are particularly relevant for high-voltage power networks, (ii) is based on analytical calculations valid for general meshed coupling networks, and (iii) considers the case of multiple sources of power feed-in noise. Our approach relies on a

single restrictive assumption, that the non-Gaussianities can be modelled by the first few cumulants of their distribution. While this excludes Lorentzian and power-law distributions with small exponents, it is not an important restriction, however, since the frequency fluctuations that have been reported in power systems so far exhibit close to exponential tails [9–12].

The manuscript is organized as follows. Following this introduction, we construct our model for the dynamics of high-voltage AC power grids in Section II. Analytical results are derived and presented in Section III. We confirm them numerically in Section IV and discuss their importance and relevance in Section V. Additional theoretical and numerical results are presented in the Appendix and the Supplemental Material.

II. THE DYNAMICAL MODEL

A. The Swing Equations

The operational state of an AC power grid is determined by complex voltages $V_i = |V_i| \exp[i\phi_i]$ at each of the $i = 1, \dots, N$ nodes of the grid. In normal operation, voltage amplitudes are fixed not far from their rated value, and voltage angles rotate close to the rated frequency, $\phi_i(t) = \Omega_0 t + \theta_i(t)$, with $\Omega_0/2\pi = 50$ or 60Hz. Over time intervals ranging roughly from seconds to several tens of seconds, the transient dynamics of high-voltage power grids is given by the swing equations [5]. They govern the time-evolution of voltage angles in a frame rotating at the rated frequency. In high-voltage power grids, a standard approximation is the lossless line approximation, which neglects Ohmic losses. The swing equations then read

$$m_i \ddot{\theta}_i + d_i \dot{\theta}_i = P_i - \sum_j B_{ij} \sin(\theta_i - \theta_j), \quad (1)$$

with the inertia (m_i) and damping (d_i) parameters. The active power P_i is positive for generators and negative for loads, and $B_{ij} = b_{ij}|V_i||V_j|$ denotes the product of the voltage magnitudes at nodes i and j with the line susceptance. If there is no line between i and j , then $b_{ij} = B_{ij} = 0$. In the lossless line approximation, line

conductances are neglected. The approximation is justified when dealing with very high-voltage power grids, which typically have $g/b < 0.1$ for the ratio of conductance over susceptance (see Supplemental Material).

At equilibrium, electric power grids are synchronized network systems [29]. They lie close to an operational synchronous state where voltage angles are solutions to a set of transcendental equations called the power flow equations. Under our assumptions, they read

$$P_i = \sum_j B_{ij} \sin(\theta_i - \theta_j). \quad (2)$$

Their solution $\{\theta_i^{(0)}\}_{i=1,\dots,N}$ corresponds to the instantaneous, synchronous operational state of the power grid.

B. Wave Propagation

We want to investigate how a local perturbation about the solution to Eq. (2) propagates across the system and influences voltage angles far away from it. Such an occurrence is illustrated for the PanTaGruEl [30] model of the synchronous grid of continental Europe in Fig. 1. Initially, the system is in a steady-state solution of Eq. (2). An abrupt power loss $P_i \rightarrow 0$, corresponding to the disconnection of a large power plant in Spain, brings the system out of equilibrium. Following that perturbation, a voltage angle wave propagates across the grid, which is represented in five consecutive color-coded snapshots in Fig. 1.

In large power grids, even the loss of large power plants is a relatively weak perturbation in a mathematical sense. For instance the European Network of Transmission System Operators for Electricity (ENTSO-E) reference incident considers the simultaneous tripping of two of the largest power plants, connected to the same bus [31]. This corresponds to less than one percent of the total power injected in the synchronous grid of continental Europe. For the case plotted in Fig. 1 of a power loss of $\Delta P = 900\text{MW}$, corresponding to a large power plant, frequency deviations never exceed $\Delta\omega/2\pi = 0.12\text{ Hz}$, i.e. a fraction of a percent of the rated frequency [17]. Power feed-in noises being by nature smaller than the rated power on which they are superimposed, it is therefore legitimate to investigate them through the linearization of Eq. (1) about the operational synchronous state. With $\theta_i = \theta_i^{(0)} + \delta\theta_i$ and $P_i = P_i^{(0)} + \delta P_i$, one gets

$$\mathbf{M}\delta\ddot{\boldsymbol{\theta}} + \mathbf{D}\delta\dot{\boldsymbol{\theta}} = \delta\mathbf{P} - \mathbf{L}\delta\boldsymbol{\theta}, \quad (3)$$

where we grouped the voltage angle deviations into a vector $\delta\boldsymbol{\theta}$, and introduced the diagonal inertia and damping matrices, $\mathbf{M} = \text{diag}(m_i)$ (with $m_i = 0$ on load nodes), $\mathbf{D} = \text{diag}(d_i)$ as well as the weighted network Laplacian matrix \mathbf{L} ,

$$\mathbf{L}_{ij} = \begin{cases} -B_{ij} \cos(\theta_i^{(0)} - \theta_j^{(0)}), & \text{for } i \neq j, \\ \sum_k B_{ik} \cos(\theta_i^{(0)} - \theta_k^{(0)}), & \text{for } i = j. \end{cases} \quad (4)$$

The perturbation generating a wave of voltage angle and frequency disturbances is encoded in the source term vector $\delta\mathbf{P}$, whose components are non-zero at nodes where the perturbation is active. Below we consider cases of (i) a single noisy perturbation and (ii) a collection of independent, geographically distributed noisy perturbations.

Power grids have two types of nodes, corresponding to power plants and loads. They have very different dynamical inertia and damping parameters. Most loads as well as inverter-connected, new renewable sources of energy have no inertia, $m_i = 0$, while traditional power plants have an inertia roughly proportional to their rated power output [5]. Furthermore, loads have a damping parameter significantly smaller than generators [32]. While it is crucial to incorporate these dynamic inhomogeneities in any analysis of realistic power grids, they render analytical approaches intractable. Recent works took a perturbation theory approach to incorporate small deviations about the homogeneous case [33, 34], however most are based on homogeneity assumptions [35–38]. To justify it, one often invokes a Kron-reduction [39] into an effective network with modified line susceptances connecting only inertiaful, generator nodes. This transformation is based on Schur's complement formula [40], and since the reduced load nodes have no inertia and a much smaller damping term, this reduction modifies the dynamics on the generators only marginally. Once the reduction is performed, one furthermore argues that considering uniform damping and inertia, $d_i = d$, $m_i = m$ is justified, because, only large plants, all with large rated power are connected to the high-voltage grids we are focusing on here. Additionally, machine measurements indicate that the ratio of damping over inertia does not vary by much from one machine to another [41]. Hence, in our analytical treatment, we consider noise propagation from Eq. (3) for a Kron-reduced network with homogeneous dynamic parameters, $d_i = d$, $m_i = m$. However, our numerical simulations are entirely free from this assumption and are based on a realistic, inhomogeneous power grid model. Our numerical results corroborate our analytical results in the particularly relevant regime of long noise correlation time.

III. DISTURBANCE WAVE PROPAGATION : ANALYTICAL APPROACH

A. Linearized swing equations and modal decomposition

Eq. (3) is a damped wave equation with a source term. It is defined on a discrete, meshed complex network encoded in the Laplacian matrix \mathbf{L} , which accordingly replaces the Laplace operator of continuous wave equations. Given a source term $\delta\mathbf{P}(t)$, we compute the moments $\mu_p \equiv \langle \delta\hat{\theta}_i^p(t \rightarrow \infty) \rangle$, $p \leq 4$ of the distribution of angle deviations at any node i on the network. Because we are interested in local fluctuations about the instan-

taneous average response, we measure angle deviations from their geographical average, $\delta\theta_i(t \rightarrow \infty) = \delta\theta_i(t \rightarrow \infty) - \Delta$ where $\Delta = N^{-1} \sum_j \delta\theta_j(t \rightarrow \infty)$. Here, $t \rightarrow \infty$ means that the observation takes place long after the onset of the noisy perturbation, to avoid transient behaviors. To shorten notations, we do not explicitly write it from now on.

To calculate $\mu_p \equiv \langle \delta\hat{\theta}_i^p \rangle$, we use a modal expansion of Eq. (3) over the set of eigenmodes $\{\mathbf{u}_\alpha\}$ of the Laplacian matrix \mathbf{L} . We first write the total angle deviation as $\delta\theta_i(t) = \sum_\alpha c_\alpha(t) u_{\alpha,i}$. Eq. (3) then gives

$$m\ddot{c}_\alpha + d\dot{c}_\alpha + \lambda_\alpha c_\alpha = \delta\mathbf{P}(t) \cdot \mathbf{u}_\alpha, \quad (5)$$

where $\mathbf{L}\mathbf{u}_\alpha = \lambda_\alpha \mathbf{u}_\alpha$, with $\lambda_\alpha \geq 0$, $\alpha = 1, \dots, N$. Because angle deviations $\delta\hat{\theta}_i(t) = \delta\theta_i(t) - \Delta(t)$ are defined relative to their geographical average $\Delta(t)$, the bulk voltage angle shift along the zero-mode $u_{1,i} = 1/\sqrt{N}$ of the Laplacian matrix is subtracted, and the rest of this manuscript considers the dynamics orthogonal to that zero-mode. This in particular removes contributions from time-dependent excursions of angle/frequency averages, which may be another source of non-Gaussianity [12].

Eq. (5) is the differential equation for a damped, driven harmonic oscillator. It is easily solved by means of Laplace transforms. The general solution reads [30]

$$c_\alpha(t) = m^{-1} e^{-(\gamma + \Gamma_\alpha)t/2} \int_0^t e^{\Gamma_\alpha t_2} \times \int_0^{t_2} e^{(\gamma - \Gamma_\alpha)t_1/2} \delta\mathbf{P}(t_1) \cdot \mathbf{u}_\alpha dt_1 dt_2, \quad (6)$$

with $\Gamma_\alpha = \sqrt{\gamma^2 - 4\lambda_\alpha/m}$ and $\gamma = d/m$. Moments μ_p of voltage angle deviations are calculated as averages over the noise distribution. From Eq. (6), μ_p contains an ensemble-average $\langle \delta P_{i_1}(t_1) \delta P_{i_2}(t_2) \dots \delta P_{i_p}(t_p) \rangle$, over the product of p sources of noise inside exponential integrals. One therefore needs to specify the moments of the noise distribution. We start from a geographically uncorrelated feed-in noise on nodes labeled i_0 , whose first two moments are given by

$$\langle \delta P_{i_0}(t_1) \rangle = 0, \quad (7a)$$

$$\langle \delta P_{i_0}(t_1) \delta P_{i_0}(t_2) \rangle = \sigma^2 e^{-|t_1 - t_2|/\tau_0}, \quad (7b)$$

to which we add non-Gaussianities in the form of finite skewness and kurtosis of the noise distribution,

$$\langle \delta P_{i_0}(t_1) \delta P_{i_0}(t_2) \delta P_{i_0}(t_3) \rangle = a_3 \sigma^3 \prod_{m < n} e^{-|t_{i_m} - t_{i_n}|/\tau_0}, \quad (8a)$$

$$\langle \delta P_{i_0}(t_1) \delta P_{i_0}(t_2) \delta P_{i_0}(t_3) \delta P_{i_0}(t_4) \rangle_c = a_4 \sigma^4 \prod_{m < n} e^{-|t_{i_m} - t_{i_n}|/\tau_0}, \quad (8b)$$

where $\langle \dots \rangle_c$ explicitly refers to a cumulant. This in particular substracts all disconnected averages such as $\langle \delta P_{i_0}(t_1) \delta P_{i_0}(t_2) \rangle \langle \delta P_{i_0}(t_3) \delta P_{i_0}(t_4) \rangle$. The parameters $a_{3,4}$ characterize non-Gaussianities in the noise distribution. They correspond to skewed distributions ($a_3 \neq 0$), with tails longer ($a_4 > 0$) or shorter ($a_4 < 0$) than the normal distribution.

The moments μ_p are given by exponential integrals and are straightforwardly calculated. However, their exact expressions are somewhat complicated. We give them for the variance only and, for the third and fourth cumulants, discuss limiting cases of long and short correlation time.

B. Time scales in high-voltage power grids vs. noise correlation time

Eq. (5) makes it clear that, beside τ_0 , the other time scales are the damping time $\gamma^{-1} = m/d$, the α^{th} oscillator period $T_\alpha = \sqrt{m/\lambda_\alpha}$ and the combination $\gamma T_\alpha^2 = d/\lambda_\alpha$ of the two [18]. For the high voltage synchronous grid of continental Europe, a detailed analysis based on realistic line admittances and dynamic parameters gave estimates for these time scales as $\gamma^{-1} \simeq 2.5s$, $T_\alpha < 1s$ and $\gamma T_\alpha^2 < 0.4s \forall \alpha$. Therefore the regime of long noise correlation time is already reached for

$\tau_0 \gtrsim 5 - 10s$, while the short correlation time regime requires $\tau_0 \lesssim 1\mu s$ [17, 18]. In between lies a hybrid regime, where disturbance time scales overlap with spectral time scales [20].

While circuit breakers and other switches may disconnect power lines and put a power plant off-line in a fraction of a second, disconnection-reconnection sequences may occur at most two to three times consecutively by design. It is hard to think of a significant noise perturbation fluctuating persistently on a time scale shorter than a few seconds. Moreover, in the Supplemental Material we show several examples of feed-in power fluctuations from renewables, which are all characterized by correlation times $\tau_0 \gtrsim 1$ min in the sense of the two-point correlator of Eq. (7b). Hence, we conclude that the long correlation time regime is the relevant one for our investigations.

We first consider the case of a single source of noise and discuss multiple noisy nodes in paragraph III F.

C. Voltage angle variance

In the limit of large observation time, the voltage angle variance is given in Eq. (S10) of the Supplemental Material. The two limiting cases of long and short noise

correlation time τ_0 give key insights on noise propagation.

First, when τ_0 is the largest time scale, the voltage angle variance at node i reads

$$\lim_{\tau_0 \rightarrow \infty} \langle \delta \tilde{\theta}_i^2 \rangle = \left(\sigma \sum_{\alpha \geq 2} \frac{u_{\alpha, i_0} u_{\alpha, i}}{\lambda_\alpha} \right)^2. \quad (9)$$

Because we consider deviations from the geographically averaged response, the sum excludes the zero-mode of the network Laplacian matrix. The quantity squared inside the parenthesis in Eq. (9) is the Green's function for the linear operator \mathbf{L} , from the noise source to the observation node i . For optical or electronic waves propagating through disordered mesoscopic systems, quantities similar to $\langle \delta \tilde{\theta}_i^2 \rangle$ in Eq. (9) decay as power laws with the distance between i_0 and i , when averaged over a relatively narrow but high-lying spectral interval [42]. Eq. (9) instead corresponds to a “zero-energy” Green's function, indicating that fluctuations with long correlation times are transmitted by a few low-lying, long-wavelength eigenmodes of \mathbf{L} , for which the perturbative approaches of Ref. [42] cannot be directly applied.

Second, when τ_0 is the shortest time scale, one obtains

$$\lim_{\tau_0 \rightarrow 0} \langle \delta \tilde{\theta}_i^2 \rangle = 2\sigma^2 \tau_0 \sum_{\alpha, \beta \geq 2} \frac{u_{\alpha, i_0} u_{\beta, i_0} u_{\alpha, i} u_{\beta, i}}{d(\lambda_\alpha + \lambda_\beta) + \frac{m}{2d}(\lambda_\alpha - \lambda_\beta)^2}. \quad (10)$$

In the inertialess limit, $m = 0$, the variance is given by a two-particle Green's function in this case.

D. Higher voltage angle cumulants : Long correlation time regime

In the limit of long correlation time, it is straightforward to show that higher cumulants behave similarly to the variance, Eq. (9), namely (see Supplemental Material Sec. II, C.)

$$\lim_{\tau_0 \rightarrow \infty} \langle \delta \tilde{\theta}_i^p \rangle_c = a_p \left(\sigma \sum_{\alpha \geq 2} \frac{u_{\alpha, i_0} u_{\alpha, i}}{\lambda_\alpha} \right)^p, \quad (11)$$

with the parameters a_p giving the deviation from Gaussianity in the feed-in fluctuations, Eqs. (8). The most remarkable thing is that, from Eqs. (9) and (11), standardized higher cumulants are given by $\langle \delta \tilde{\theta}_i^p \rangle_c / \langle \delta \tilde{\theta}_i^2 \rangle^{p/2} = a_p$, regardless of the distance between the measured node and the noise source. This is one of the main results of this paper: long correlation times enable non-Gaussian fluctuations from a single noise source to propagate over the whole network and persist at their initial relative value compared to the variance, i.e. to Gaussian fluctuations. This result is in particular independent of inertia, suggesting, as previously found in Ref. [43], that disturbances with long characteristic times are affected only marginally by inertia, even when the latter is inhomogeneously distributed. This independence of inertia makes sense since in the long-correlation time limit the system

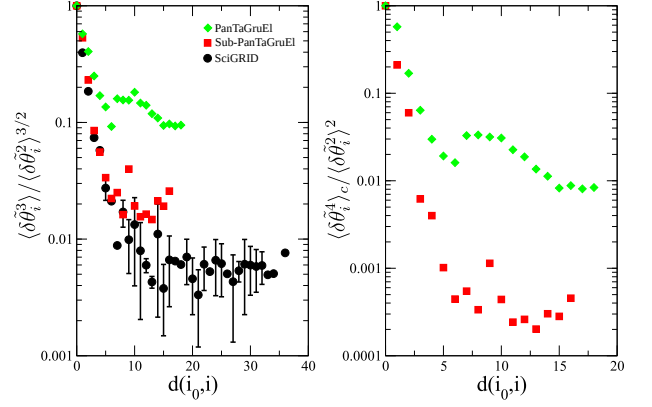


FIG. 2. Left panel: Normalized ratio $\langle \delta \tilde{\theta}_i^3 \rangle / \langle \delta \tilde{\theta}_i^2 \rangle^{3/2}$ in the limit of short correlation time, given by Eqs. (S4) and (S8) in the Supplemental Material. Right panel: Normalized voltage angle kurtosis $\langle \delta \tilde{\theta}_i^4 \rangle_c / \langle \delta \tilde{\theta}_i^2 \rangle^2$ in the limit of short correlation time and in the absence of inertia, given by Eqs. (S4) and (S9). Data are plotted as a function of the geodesic distance $d(i_0, i)$ between the measurement node i and the noise source node i_0 . Black symbols correspond to the full PanTaGruEl model of the synchronous grid of continental Europe [17, 18], red symbols to a connected subsection with $N=1000$ nodes of PanTaGruEl and green ones to the SciGRID model of the high voltage power grid of Germany [44]. Error bars indicate the data spread for different measurements at the same geodesic distance. PanTaGruEl data for the kurtosis are missing because they require prohibitively large computation times.

response simply tracks the equilibrium point of Eq. (2) with perturbed power inputs. Large voltage angle fluctuations are therefore boosted by finite-time correlated disturbances. We stress that, as defined in Section III A, Eq. (11) refers to voltage angle deviations from their geographical average. Therefore, the network-wide propagation of non-Gaussianities predicted by Eq. (11) goes beyond the bulk response reported in Refs. [20] and [7].

E. Higher voltage angle cumulants : Short correlation time regime

In the limit of short τ_0 , the third moment of voltage angles is given in Eq. (S11) in the Supplemental Material. In the limit of vanishing inertia, $m = 0$, it gives,

$$\lim_{\tau_0 \rightarrow 0} \langle \delta \tilde{\theta}_i^3 \rangle = \sigma^3 \tau_0^2 \sum_{\alpha, \beta, \gamma \geq 2} \frac{u_{\alpha, i_0} u_{\beta, i_0} u_{\gamma, i_0} u_{\alpha, j} u_{\beta, j} u_{\gamma, j}}{d^2(\lambda_\alpha + \lambda_\beta + \lambda_\gamma)}, \quad (12)$$

which, together with Eq. (10), reflects the fact that, for Kuramoto, i.e. inertialess oscillators, non-Gaussianities in the p^{th} cumulants propagate as a p -particle Green's function in the white-noise limit.

As mentioned previously, Green's functions decay exponentially with distance in disordered mesoscopic systems [42], however it is not clear whether this behavior applies to the “zero-energy” case considered here, nor to p -particle Green's functions. To understand better the

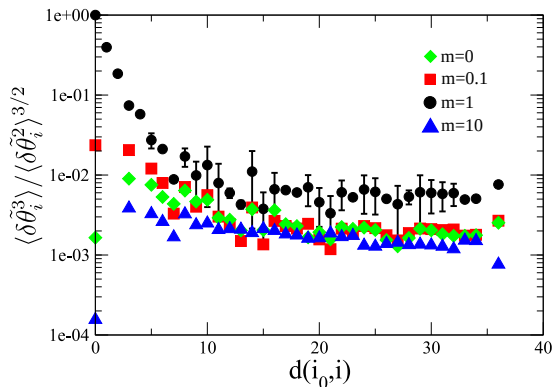


FIG. 3. Normalized ratio $\langle \delta \tilde{\theta}_i^3 \rangle / \langle \delta \tilde{\theta}_i^2 \rangle^{3/2}$ in the limit of short correlation time, given by Eqs. (S10) and (S11) in the Supplemental Material, as a function of the geodesic distance $d(i_0, i)$ between the measurement node i and the noise source node i_0 . Data correspond to the full PanTaGruEl model of the synchronous grid of continental Europe [17, 18] without inertia (black), with $m = 0.1$ (red) $m = 1$ (green) and $m = 10$ (blue). Data are normalized such that the inertialess case goes to one as the geodesic distance goes to zero. Error bars indicate the data spread for different measurements at the same geodesic distance.

propagation of non-Gaussianities in the short correlation time regime, we therefore numerically evaluate the expressions in Eqs. (10) and (12). First, Fig. 2 shows the theoretically predicted standardized skewness and kurtosis (normalized by a_3 and a_4 respectively) for inertialess networks, as a function of the geodesic distance to the source of noise, for various power grid models. In contrast to the long correlation time prediction, both skewness and kurtosis decay fast away from the noisy node (seemingly exponentially fast) before they saturate at a constant, small value. This means that, for inertialess networks subjected to fast-varying noise, skewness and kurtosis exhibit an additional decay, on top of the exponential decay of the angle variance reported in Refs. [9, 20].

It is well known that inertia plays an important role in absorbing fast fluctuating disturbances with short correlation time. Therefore, we further show in Fig. 3 the standardized kurtosis as predicted by the formulae of Eqs. (S10) and (S11), for various values of inertia. As inertia increases, the kurtosis is further suppressed compared to the variance. The influence is especially strong a short distance away from the noise source. This agrees with numerical data reported in Ref. [9] and corroborates earlier findings that inertia impacts the dynamics mainly locally and at short times [43].

The data presented in Fig. 2 and 3 show that short noise correlation times suppress the propagation of non-Gaussian voltage angle fluctuations through meshed networks over a network-dependent distance. This is an additional effect, further suppressing non-Gaussianities relative to the already decaying voltage angle variance. The effect becomes stronger at larger inertia. Note also

that the grid models used in Figs. 2 and 3 fairly capture the parameters of actual high-voltage power grids.

F. Multiple sources of noise

We finally consider the case with M distinct, independently but identically distributed sources of power feed-in fluctuations. In that case, there are M contributions similar to that in Eq. (11), but $M!(M-p/2)!/(p/2)!$ pairings of the noise sources for the moment of even order p . These latter contributions are much more numerous and they result in a Gaussian p^{th} moment – this is the standard mechanism behind central limit and Berry-Esseen theorems [45]. For instance for the $p = 4$ moment in the large correlation time limit, one obtains

$$\lim_{\tau_0 \rightarrow \infty} \langle \delta \tilde{\theta}_i^4 \rangle = \sum_{i_0=1}^M \left(\sigma \sum_{\alpha \geq 2} \frac{u_{\alpha, i_0} u_{\alpha, i}}{\lambda_{\alpha}} \right)^4 + 3 \sum_{i_0 \neq j_0} \left(\sigma \sum_{\alpha \geq 2} \frac{u_{\alpha, i_0} u_{\alpha, i}}{\lambda_{\alpha}} \right)^2 \left(\sigma \sum_{\beta \geq 2} \frac{u_{\beta, j_0} u_{\beta, i}}{\lambda_{\beta}} \right)^2, \quad (13)$$

where the factor 3 in the second line accounts for all pos-

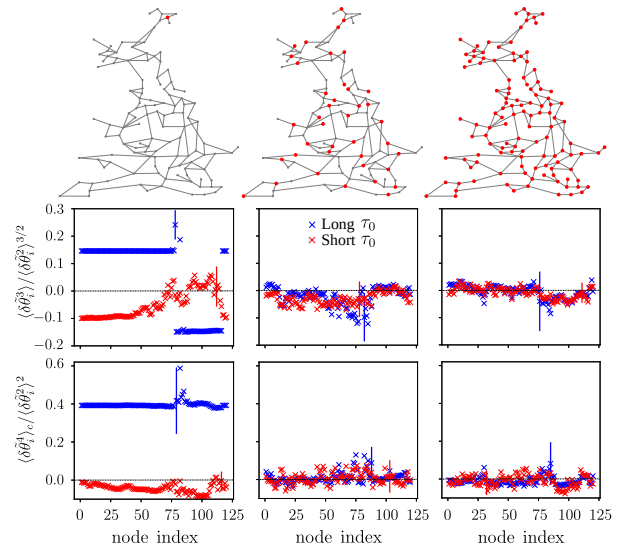


FIG. 4. Numerically evaluated voltage angle skewness and kurtosis for the UK high voltage power grid with realistic, i.e. inhomogeneous damping and inertia parameters and 1 (left column), 40 (middle) and 120 (right) sources of noise, whose locations are shown in the grid map in the top panels. Blue (red) crosses correspond to noise with long (short) correlation time. Error bars are indicated on nodes that have the largest numerical fluctuation when doubling the simulation time. Injected noises have skewness and kurtosis with $a_3 = -0.15$ and $a_4 = 0.4$ for long correlation time and $a_3 = -1.4$ and $a_4 = 18.9$ for short correlation time.

sible pairings between the product of four noise sources, δP_{i_l} , $l = 1, \dots, 4$. The pairing mechanism giving the second term on the right-hand side of Eq. (13) leads to the

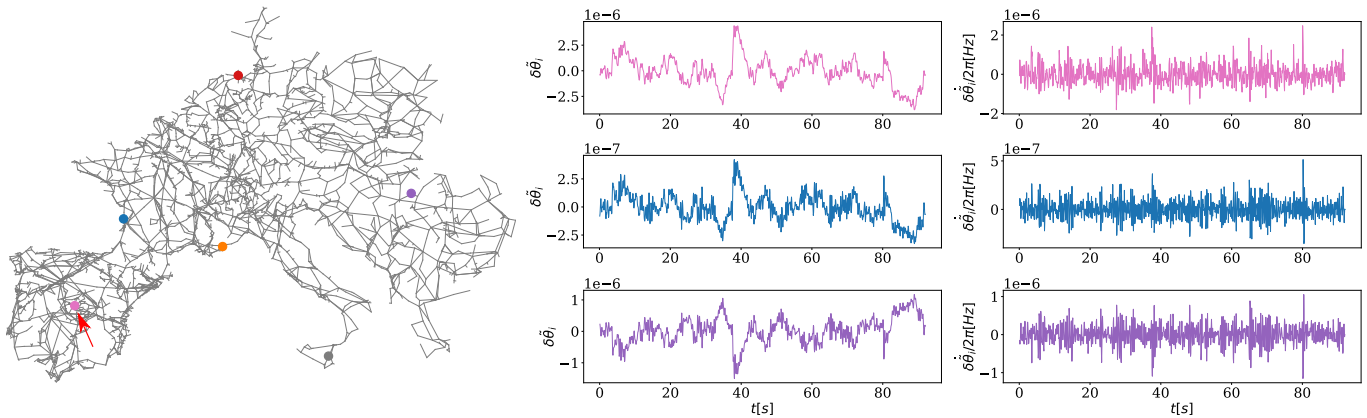


FIG. 5. Left panel: map of the PanTaGruEl model of the synchronous grid of continental Europe, with 3809 nodes connected by 4944 power lines [17, 18]. Center and right panels: time series for voltage angle (center) and frequency (right) generated by a single non-Gaussian source of noise for the PanTaGruEl model with inhomogeneous inertia and damping. Noise in the regime of long correlation time is injected at the pink node indicated by the red arrow in the left panel. Voltage angle and frequency deviations are measured at the colored nodes and time sequences for the pink, blue and violet nodes are shown. Time series for the orange, red and grey nodes are shown in Fig. S1 in the Supplemental Material

convergence of the voltage angle distribution to a Gaussian distribution, with $\langle \delta\theta_i^4 \rangle / \langle \delta\theta_i^2 \rangle^2 \rightarrow 3$ [to see this, sum over the noisy nodes $i_0 = 1, \dots, M$ in Eq. (11) and compare the result with (13)]. The convergence is the same as in the Berry-Esseen theorem [45]. When M is large, this second term dominates over the first one by a factor $(M-1)/2$, so that the ratio of the fourth cumulant – a measure of non-Gaussianity – to the fourth moment becomes $\propto M^{-1}$. With the standard definition [45], non-Gaussianities disappear at a rate $\propto M^{-1/2}$.

IV. NUMERICAL RESULTS

We numerically confirm our analytical results and extend them to voltage frequency distributions, the latter being of direct interest for electric power grids.

Our two main theoretical predictions are that,

(i) non-Gaussianities propagate over the entire network just like Gaussian fluctuations, when they originate from a noisy source with long correlation time. They disappear exponentially with the distance from the source for short noise correlation time,

(ii) non-Gaussianities become smaller with the number M of uncorrelated sources of noise. We confirm these two predictions by numerical integration of Eq. (1) for various networks with single or multiple sources of noise with short and long correlation times.

Fig. 4 first illustrates how voltage angle fluctuations behave as more uncorrelated sources of noise are added. Blue and red crosses correspond to long and short noise correlation times respectively, and three situations of a single (left column), 40 (middle) and 120 (right) uncorrelated sources of noise are shown. When a single noise source is present, skewness and kurtosis of voltage angles directly reflect their value for the noise source for

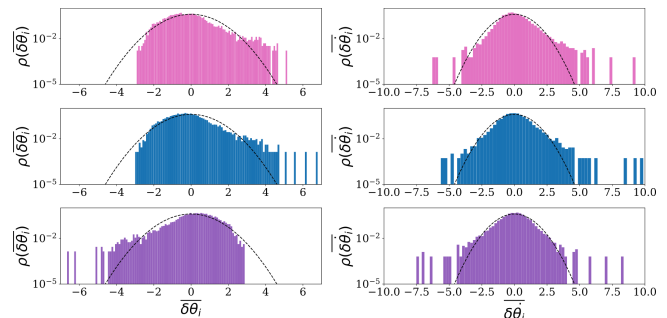


FIG. 6. Normalized distributions of voltage angles $\overline{\delta\theta}_i = \delta\theta_i / \sqrt{\langle \delta\theta_i^2 \rangle}$ (left panels) and frequencies $\overline{\delta f}_i = \delta f_i / \sqrt{\langle \delta f_i^2 \rangle}$ (right panels), from a single non-Gaussian source of noise in PanTaGruE, with homogeneous inertia and damping parameters. All normalized distributions are the same, up to a sign inversion, in agreement with our analytical prediction of Eq. (11). Dashed lines indicate a Gaussian distribution. Colors refer to the colored nodes in the left panel of Fig. 5, and distributions for the orange, red and grey nodes are shown in Fig. S2 in the Supplemental Material. Voltage angle distributions retain their non-Gaussianity regardless of the distance to the disturbance, in agreement with our predictions of Eq. (11).

long noise correlation time, while they are significantly reduced for short correlation time. In the latter case, a finite skewness persists over more than half of the network, and fluctuates about zero for the rest of the network nodes. As the number of noise sources increases, both skewness and kurtosis are suppressed as voltage angles become normally distributed following the action of the Berry-Esseen theorem. Numerical data still fluctuate due to the discreteness of time steps and the finiteness of the integration time. Error bars indicate the largest data variation upon doubling of the integration time.

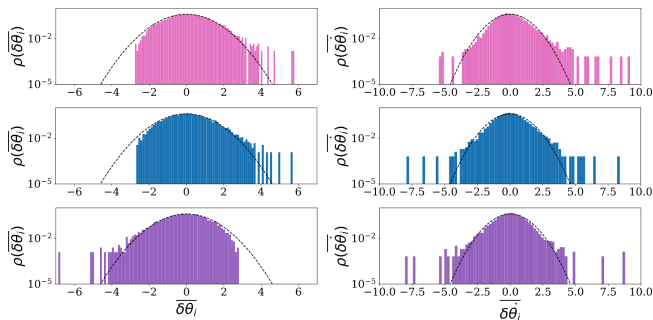


FIG. 7. Normalized distributions of voltage angles $\overline{\delta\theta}_i = \delta\theta_i/\sqrt{\langle\delta\theta_i^2\rangle}$ (left panels) and frequencies $\overline{\delta\omega}_i = \delta\omega_i/\sqrt{\langle\delta\omega_i^2\rangle}$ (right panels), as in Fig. 6, but for an inhomogeneous, realistic configuration of inertia and damping of the PanTaGruEl model. Colors refer to the colored nodes in the left panel of Fig. 5. Distributions for the orange, red and grey nodes are shown in Fig. S3 in the Supplemental Material. Voltage angle distributions retain their non-Gaussianity regardless of the distance to the disturbance, in agreement with our predictions of Eq. (11).

A remarkable feature in Fig. 4 is the sign change in the long-correlation-time skewness in the middle-left panel. It is easily understood when re-expressing the single-particle Green's function in terms of graph theoretic indicators as

$$\sum_{\alpha \geq 2} \frac{u_{\alpha,i_0} u_{\alpha,i}}{\lambda_{\alpha}} = -\frac{1}{2} [\Omega_{i_0,i} - C_1^{-1}(i_0) - C_1^{-1}(i) + 2Kf_1/n^2], \quad (14)$$

where $\Omega_{i_0,i}$ is the resistance distance between node i_0 and i [46], $C_1(i) = (n^{-1} \sum_j \Omega_{ij})^{-1}$ is the resistance centrality of node i and $Kf_1 = \sum_{i < j} \Omega_{i,j}$ is the so-called Kirchhoff index [46, 47]. The sign of all odd- p cumulants in the long correlation time limit, see Eq. (11), is given by the p^{th} power of the Green's function. It is therefore determined by a trade-off between the centralities of the input and measured nodes on the one hand, and the resistance distance between them on the other hand. As but one consequence, the skewness changes sign as the measurement point i is taken further and further away from i_0 , when the resistance distance $\Omega_{i_0,i}$ becomes larger than the sum of the inverse node centralities in Eq. (14). Theory-simulation agreement for the UK model is excellent, and well within the error bars of finite-time integration.

We next turn our attention to a larger-scale, more realistic model of a high-voltage power grid and consider the PanTaGruEl model of the synchronous grid of continental Europe [17, 18]. As discussed in Section III B, intrinsic time scales in such large-scale power grids are such that the short correlation time limit corresponds to $\tau_0 \lesssim 1\mu\text{s}$ while the long correlation time regime corresponds to $\tau_0 \gtrsim 5 - 10\text{s}$. Persistent sources of noise therefore correspond to the long correlation time regime, which we focus on.

Figs. 5 shows data for an inhomogeneous high-voltage

power grid with realistically distributed inertia (m_i) and damping (d_i) parameters in Eq. (1). A non-Gaussian power feed-in noise is injected at the pink node indicated by the red arrow on the network map (left panel), and voltage angle as well as frequency fluctuations are measured at the colored nodes. Time series for voltage angles and frequencies are shown, which fluctuate differently in magnitude, depending on the measurement location. In the considered regime of long correlation time, the response is inhomogeneous and distinct from the bulk response discussed in [20], where all nodes have the same voltage angles and frequencies response.

We focus on voltage angle and frequency distributions in Figs. 6–8. One sees first in Fig. 6, that all voltage angle and frequency distributions are the same, up to a sign inversion $\delta\tilde{\theta}_i \rightarrow -\delta\tilde{\theta}_i$, in the homogeneous case of constant inertia and damping, $m_i = m$ and $d_i = d$ in Eq. (1). This corroborates our prediction of Eq. (11), according to which all standardized cumulants are the same, up to possible sign changes in odd cumulants, in the case of noise with long correlation time. The observed sign change is consistent with Eq. (14), where the blue node has the same normalized voltage angle distribution as the source, pink node, because it is close to it and the right-hand side in Eq. (14) is dominated by the sum of the inverse centralities, $C_1^{-1}(i_0) + C_1^{-1}(i) > \Omega_{i_0,i}$. All other nodes are further away and correspond to a regime where the inequality is reversed, $C_1^{-1}(i_0) + C_1^{-1}(i) < \Omega_{i_0,i}$ and odd cumulants undergo a sign change. Note the different magnitude of fluctuations for voltage angle and frequency trajectories in the different panels of Fig. 5.

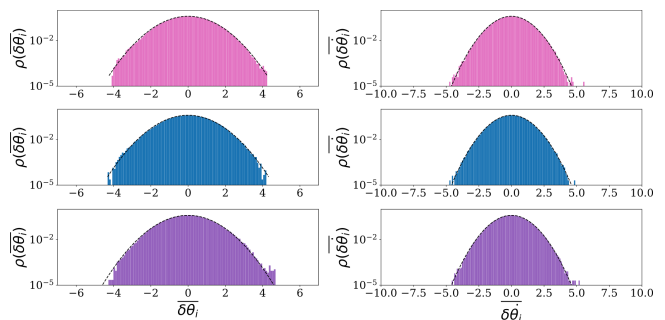


FIG. 8. Normalized distributions of voltage angles $\overline{\delta\theta}_i = \delta\theta_i/\sqrt{\langle\delta\theta_i^2\rangle}$ (left panels) and frequencies $\overline{\delta\omega}_i = \delta\omega_i/\sqrt{\langle\delta\omega_i^2\rangle}$ (right panels), as in Fig. 7, but for 381 different, uncorrelated sources of non-Gaussian noise in the PanTaGruEl model. Colors refer to the colored nodes in the left panel of Fig. 5. Distributions for the orange, red and grey nodes are shown in Fig. S4 in the Supplemental Material.

In the regime of long correlation time, we saw in Section III D that voltage angle cumulants depend neither on inertia, nor on damping, and following Ref. [43] we conjectured that the prediction of Eq. (14) also applies to cases with inhomogeneous inertia and damping. We confirm this conjecture in Fig. 7, where the normalized voltage angle and frequency distributions also keep their

non-Gaussianities all over the network, *regardless of the distance between source and measurement nodes*, in the PanTaGruEl model with realistically inhomogeneous dynamic parameters m_i and d_i .

Finally, we investigate the case when multiple uncorrelated sources of noise are present. Fig. 8 confirms that, for 381 sources of power feed-in fluctuations, non-Gaussianities disappear and both voltage angle and frequency deviations become Gaussian distributed. These numerical simulations with realistic models of high-voltage power grid fully confirm the theoretical predictions presented in Section III.

V. CONCLUSION

The theory presented has uncovered two previously neglected, yet crucial characteristics determining how voltage angle and frequency disturbances propagate through power grids: the correlation time τ_0 (i.e. the characteristic time over which sources fluctuate) and the number of sources of fluctuations. First, we show that non-Gaussian fluctuations decay with the distance from the source faster than Gaussian fluctuations do in the white-noise limit of short τ_0 . Such white-noise fluctuations eventually saturate at small values, which are determined by, e.g., the relevant multi-particle Green's function in the limit of small inertia. Second, in the other limit of long correlation times, non-Gaussian noise propagates through the whole network, regardless of the distance to the source and independently of inertia, leading to voltage angle fluctuations with the same non-Gaussian distribution as the feed-in power noise. Such large-scale propagation has been observed in frequency measurement over the Continental European grid (See Fig.6 in [10]). Third, these non-Gaussianities disappear, in the presence of multiple, uncorrelated sources due to the action of a Berry-Esseen/central limit theorem.

Modern power grids are rather resilient and in particular able to absorb moderate voltage angle fluctuations

in a normal operational mode. Yet, future grids will be subjected to more disturbances, especially from new renewable energy sources. As such, a major planification and operational concern is that electro-mechanical inertia may be significantly reduced at times of large renewable power production. While inertia reduction clearly poses a number of challenges from the point of view of short-range and/or short-time absorption of disturbances, our results indicate that, from the point of view of mid- to long-range disturbance propagation, the effects of inertia are small for the correlation-time regime relevant for renewable energy sources. Indeed, significant fluctuations in the power feed-in of large wind or solar farms typically happen over a few seconds, which is slow compared to the grid time scales. Fluctuations on shorter time scales may originate from local control, faults or changes in the consumption, which according to our results will remain local.

We finally point out that our results on noise propagation originating from correlated and multiple sources of fluctuations should be generally applicable to diffusively coupled agent systems, well beyond the power grid and phase-oscillator models described in detail in this work.

Future works should consider a in-depth comparison between our results and voltage measurements on high-voltage power grids.

ACKNOWLEDGMENTS

PJ and MT were supported by the Swiss National Science Foundation under grant No. 200020_182050. MT was supported by the Laboratory Directed Research and Development program of Los Alamos National Laboratory under project number 20220797PRD2 and 20220774ER. JH was supported through the U.S Naval Research Laboratory Karles Fellowship. We thank Julian Fritzsche for discussions on the manuscript, Laurent Pagnier for Fig. 1 and general discussions, and Will Holmgren and Tucson Electric Power for data on photovoltaic and wind turbine productions.

-
- [1] *Climate Change and Land: an IPCC special report on climate change, desertification, land degradation, sustainable land management, food security, and greenhouse gas fluxes in terrestrial ecosystems*, Tech. Rep. (IPCC, 2019).
 - [2] J. Fleming, *Historical Perspectives on Climate Change* (Oxford University Press, Oxford, England, 1998).
 - [3] *Power systems of the future: The case for energy storage, distributed generation, and microgrids.*, Tech. Rep. (IEEE Smart Grid, 2012).
 - [4] P. Milan, M. Wächter, and J. Peinke, Phys. Rev. Lett. **110**, 138701 (2013).
 - [5] J. Machowski, J. W. Bialek, and J. R. Bumby, *Power System Dynamics*, 2nd ed. (Wiley, Chichester, U.K, 2008).
 - [6] A. Ulbig, T. S. Borsche, and G. Andersson, IFAC Proceedings Volumes **47**, 7290 (2014).
 - [7] S. Auer, F. Hellmann, M. Krause, and J. Kurths, Chaos **27**, 127003 (2017).
 - [8] B. Schäfer, M. Matthiae, X. Zhang, M. Rohden, M. Timme, and D. Witthaut, Phys. Rev. E **95**, 060203(R) (2017).
 - [9] H. Haehne, K. Schmietendorf, S. Tamrakar, J. Peincke, and S. Kettmann, Phys. Rev. E **99**, 050301 (2019).
 - [10] L. Rydin Gorjão, R. Jumar, H. Maass, V. Hagenmeyer, G. Yalcin, J. Kruse, M. Timme, C. Beck, D. Witthaut, and B. Schäfer, Nature Communications **11**, 1 (2020).
 - [11] L. Rydin Gorjão, B. Schäfer, D. Witthaut, and C. Beck, N. J. Phys. **23**, 073016 (2021).

- [12] B. Schäfer, C. Beck, K. Aihara, D. Witthaut, and M. Timme, *Nat. Energy* **3**, 119 (2018).
- [13] M. Anvari, G. Lohmann, M. Wächter, P. Milan, E. Lorenz, D. Heinemann, M. R. R. Tabar, and J. Peinke, *N. J. Phys.* **18**, 063027 (2016).
- [14] M. Wolff, K. Schmietendorf, P. Lind, O. Kamps, J. Peinke, and P. Maass, *Chaos* **29**, 103149 (2019).
- [15] M. Siami and N. Motee, *IEEE Trans. Automat. Contr.* **61**, 4055 (2016).
- [16] S. Kettemann, *Phys. Rev. E* **94**, 062311 (2016).
- [17] L. Pagnier and P. Jacquod, *PLoS ONE* **14**, 1 (2019).
- [18] M. Tyloo, L. Pagnier, and P. Jacquod, *Sci. Adv.* **5**, eaaw8359 (2019).
- [19] L. Tumash, S. Olmi, and E. Schöll, *Chaos* **29**, 123105 (2019).
- [20] X. Zhang, S. Hallerberg, M. Matthiae, D. Witthaut, and M. Timme, *Science Advances* **5**, eaav1027 (2019).
- [21] M. Schröder, X. Zhang, J. Wolter, and M. Timme, *IEEE Transactions on Network Science and Engineering* **7**, 1019 (2020).
- [22] X. Zhang, D. Witthaut, and M. Timme, *Phys. Rev. Lett.* **125**, 218301 (2020).
- [23] D. A. Wiley, S. H. Strogatz, and M. Girvan, *Chaos* **16**, 015103 (2006).
- [24] D. Witthaut and M. Timme, *Phys. Rev. E* **92**, 032809 (2015).
- [25] Y. Yang, T. Nishikawa, and A. Motter, *Science* **358**, eaan3184 (2017).
- [26] L. DeVille, *Nonlinearity* **25**, 1473 (2012).
- [27] M. Tyloo, R. Delabays, and P. Jacquod, *Phys. Rev. E* **99**, 062213 (2019).
- [28] J. Hindes, P. Jacquod, and I. B. Schwartz, *Phys. Rev. E* **100**, 052314 (2019).
- [29] A. Arenas, A. Díaz-Guilera, J. Kurths, Y. Moreno, and C. Zhou, *Phys. Rep.* **469**, 93 (2008).
- [30] M. Tyloo and P. Jacquod, *Phys. Rev. E* **100**, 032303 (2019).
- [31] ENTSO-E, Frequency Stability Evaluation Criteria for the Synchronous Zone of Continental Europe, <https://docs.entsoe.eu/dataset/inertia-report-continental-europe/> (2016).
- [32] A. R. Bergen and D. J. Hill, *IEEE Transaction on Power Apparatus and Systems* **PAS-100**, 25 (1981).
- [33] L. Pagnier and P. Jacquod, *IEEE Access* **7**, 145889 (2019).
- [34] J. Fritzsche and P. Jacquod, *IEEE Access* **10**, 19986 (2022).
- [35] E. Tegling, B. Bamieh, and D. F. Gayme, *IEEE Trans. Control Net. Syst.* **2**, 254 (2015).
- [36] F. Paganini and E. Mallada, *55th Annual Allerton Conference on Communication, Control, and Computing*, 324 (2017).
- [37] B. K. Poolla, S. Bolognani, and F. Dörfler, *IEEE Trans. Automat. Contr.* **62**, 6209 (2017).
- [38] T. W. Grunberg and D. F. Gayme, *IEEE Tran. Control Net. Syst.* **5**, 456 (2018).
- [39] G. Kron, *Tensor Analysis of Networks* (Wiley, 1939).
- [40] R. A. Horn and C. R. Johnson, *Matrix Analysis* (Cambridge University Press, New York, 1986).
- [41] G. Kou, S. Hadley, P. Markham, and Y. Liu, *Developing generic dynamic models for the 2030 eastern interconnection grid*, Tech. Rep. (Oak Ridge National Laboratory, 2012).
- [42] E. Akkermans and G. Montambaux, *Mesoscopic Physics of Electrons and Photons* (Cambridge University Press, 2007).
- [43] M. Tyloo and P. Jacquod, *IEEE Control Syst. Lett.* **5**, 929 (2021).
- [44] W. Medjroubi, C. Matke, and D. Kleinhans, *SciGRID - an Open Source Reference Model of European Transmission Networks for Scientific Analysis* - <http://scigrd.de> (2014).
- [45] R. Durrett, *Probability: Theory and Examples*, 5th ed. (Cambridge University Press, 2019).
- [46] D. J. Klein and M. Randić, *J. Math. Chem.* **12**, 81 (1993).
- [47] M. Tyloo, T. Coletta, and P. Jacquod, *Phys. Rev. Lett.* **120**, 084101 (2018).